nature photonics

LETTERS

PUBLISHED ONLINE: 4 APRIL 2010 | DOI: 10.1038/NPHOTON.2010.79

Exciton–polariton spin switches

A. Amo[1]*, T. C. H. Liew[2], C. Adrados[1], R. Houdré[3], E. Giacobino[1], A. V. Kavokin[4,5] and A. Bramati[1]*

Integrated switching devices comprise the building blocks of ultrafast optical signal processing[1,2]. As the next stage following intensity switching[1,3,4], circular polarization switches[5–9] are attracting considerable interest because of their applications in spin-based architectures[10]. They usually take advantage of nonlinear optical effects, and require high powers and external optical elements. Semiconductor microcavities provide a significant step forward due to their low-threshold, polarization-dependent, nonlinear emission[11,12], fast operation[13] and integrability. Here, we demonstrate a non-local, all-optical spin switch based on exciton–polaritons in a semiconductor microcavity. In the presence of a sub-threshold pump laser (dark regime), a tightly localized probe induces the switch-on of the entire pumped area. If the pump is circularly polarized, the switch is conditional on the polarization of the probe, but if it is linearly polarized, a circularly polarized probe fully determines the final polarization of the pumped area. These results set the basis for the development of spin-based logic devices, integrated in a chip[14].

The development of integrated optoelectronic devices relies on three fundamental elements: switching, transport and low-level logic (AND, OR and so on)[1]. Particularly promising for use in logic operations are the spin-based architectures[10]. For such devices to be competitive, very high potential commutation speeds are required, together with integrability at the micrometre scale. In the case of polarization switching, all-optical schemes present the fastest results, with switching rates in the picosecond range[5–7,9]. However, such arrangements require external polarization optics, preventing their integrability, and very high switching energies because they rely on nonlinear spin-dependent effects of limited efficiency.

Optoelectronic devices based on excitons partially solve the problem of integrability, and transistor operation[15], switching[16] and spin transport[17] have recently been demonstrated in a chip. However, schemes based on exciton propagation operate at low speeds, limited by slow exciton diffusion, which is a result of their large mass[18]. Typical switching times are on the order of ∼0.4 ns (for the exciton transistor[15]).

Exciton–polaritons combine the best features of photonic and excitonic systems, demonstrating a qualitative improvement in terms of scalability, reduced power of operation, speed and potential use in logic devices. Polaritons are mixed light–matter quasiparticles that arise from the strong coupling between photons and excitons in a micrometre-sized cavity with embedded quantum wells. Their very low mass ($\sim 10^{-4}$ times that of the electron, inherited from their photonic component) enables their propagation over long distances at very high speeds (∼1% the speed of light, on the order of $1-2\ \mu m\ ps^{-1}$), with a controlled direction determined by the momentum of the excitation laser[13,19]. Their excitonic component results in strong polariton–polariton interactions, giving rise to very high nonlinearities[20–23].

Additionally, polaritons are spin degenerate, with two possible values of spin projection on the structure axis, either $s_z = +1$ or $s_z = -1$. These spin projections directly couple to circularly polarized light (σ^+ and σ^-, respectively) in both excitation and emission, enabling the use of polaritons in polarization-sensitive devices[14,22,24]. In this Letter, we show that non-local spin switches working at very low power can be achieved in semiconductor microcavities thanks to spin-dependent nonlinear polariton–polariton interactions. The motion of polaritons results in large propagations of the switched area with a spin state determined by that of a localized probe (non-local action), potentially working at high rates due to the large polariton velocity[13,25] and reduced lifetime (in the picosecond range).

The principle of operation of polariton spin switches is as follows. The system is pumped by an external continuous-wave (c.w.) laser at low power, the wavelength of which is slightly blue-detuned from the energy of a given polariton state in the lower polariton branch (see inset in Fig. 1a). This is the off state, characterized by a low polariton population, low blueshift and low (non-resonant) absorption (point I in Fig. 1a). When the power is increased, polariton–polariton interactions renormalize the energy of the system, bringing the polariton branch into resonance with the initially blue-detuned pumping laser. This is the on state (point II in Fig. 1a), corresponding to a high polariton population and a strong nonlinear emission.

The emission curve depicted in Fig. 1a corresponds to polaritons with a given spin ($s_z = +1$) excited by circularly polarized light (σ^+). If the system is pumped to point I with a σ^+ excitation, only a σ^+ probe will be able to switch it to point II (circular polarization switch). This is a consequence of the much stronger interaction between polaritons with parallel spins than between polaritons with antiparallel spins (a ratio of 10:1)[14,26]. Polarization control of the emission can be obtained if the pump is linearly polarized (that is, in an equal-amplitude superposition of $s_z = +1$ and $s_z = -1$ polaritons). In this case, a circularly polarized probe will switch the system to the on state (point II) only for polaritons with the same polarization as that of the probe.

The rapid polariton motion allows for the switches to be non-local[27,28]. This effect is outlined in one dimension in Fig. 1b. In the left panel, a c.w. probe is turned on at a localized area within the pump spot. Originally, only that area is switched to the on state (point II in Fig. 1a), resulting in an appreciable energy renormalization. Polaritons excited in that area, which have a well-defined momentum given by the angle of incidence of the excitation laser (see Supplementary Information), rapidly move out, inducing the renormalization and switching of the rest of the spot (right panel of Fig. 1b) in a timescale dictated

[1]Laboratoire Kastler Brossel, Université Pierre et Marie Curie, École Normale Supérieure and CNRS, UPMC Case 74, 4 place Jussieu, 75252 Paris Cedex 05, France, [2]Institute of Theoretical Physics, École Polytechnique Fédérale de Lausanne, CH-1015, Lausanne, Switzerland, [3]Institut de Physique de la Matière Condensée, Faculté des Sciences de Base, bâtiment de Physique, Station 3, EPFL, CH-1015 Lausanne, Switzerland, [4]Dipartimento di Fisica, Universita di Roma II, 1, via della Ricerca Scientifica, 00133, Roma, Italy, [5]Physics and Astronomy School, University of Southampton, Highfield, Southampton, SO17 1BJ, UK. *e-mail: alberto.amo@spectro.jussieu.fr; bramati@spectro.jussieu.fr

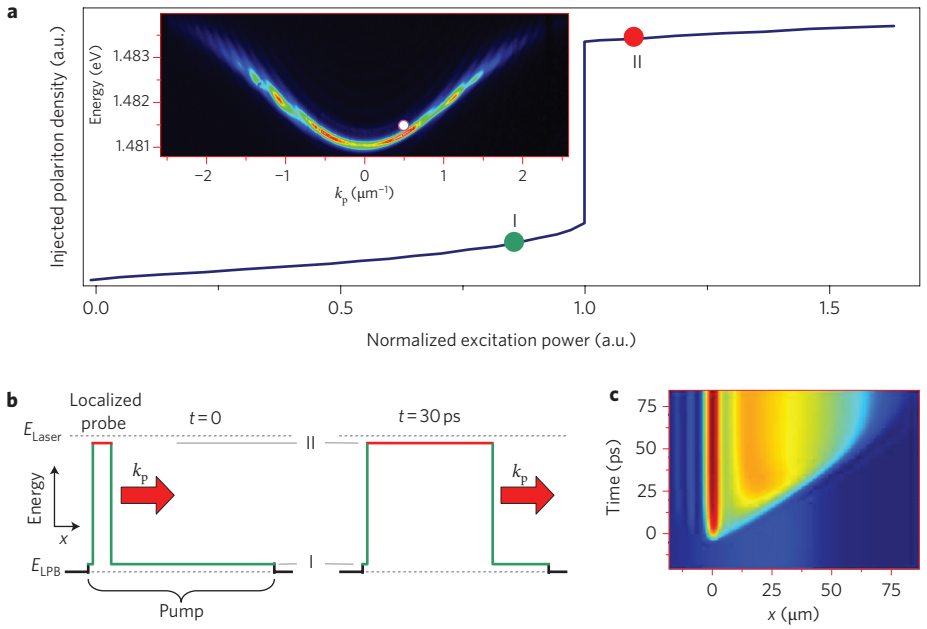

Figure 1 | Polariton dispersion, nonlinear transmission and propagation mechanism. a, Predicted spin-up polariton density variation as a function of σ^+ excitation power for an angle of incidence of 3.8° and photon energy E_{laser} slightly blue-detuned with respect to the lower polariton branch energy at low density, E_{LPB} (point I; $E_{laser} - E_{LPB} = 0.16$ meV). These excitation conditions are indicated by the white dot in the lower polariton branch dispersion shown in the inset. **b**, Sketch of our model for propagation of the switching. When the probe is turned on, it drives the system to point II only at the probe arrival area, inducing its blueshift (left part of the figure). Because of the motion of polaritons with a well-defined momentum k_p determined by the angle of incidence of the pump laser (from left to right in this case), the high-density area propagates until the rest of the pumped spot is switched *on* into the nonlinear emission regime (right part of the figure). **c**, Emitted intensity calculated from the numerical solution of the Gross–Pitaevskii equations in the conditions of the presented experiments, showing the propagation of the high-emission area along the *x*-axis as a function of time after the turn on of a σ^+ c.w. probe on the edge of a σ^+ c.w. pump spot with a diameter of 60 μm.

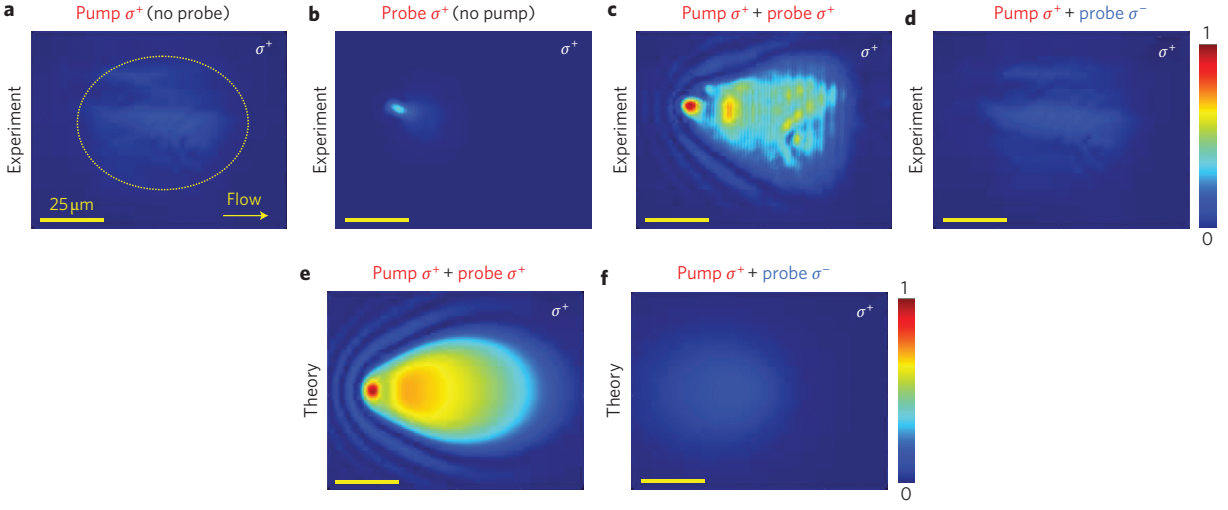

Figure 2 | Circular polarization switch (σ^+ pump). a–d, Experimental real-space images of the near-field σ^+ emission. **c**, Result of the combined effect of co-circularly polarized pump and probe (both σ^+), which are shown individually in **a**,**b. d**, When the probe polarization is changed to the cross-circular polarization (σ^-), no enhancement of the absorption/emission is observed. **e**,**f**, Results from the numerical solution of the Gross–Pitaevskii equations, corresponding to the conditions of **c** and **d**, respectively. The *z*-scale is kept constant in all panels. The dotted line in **a** depicts the extension of the pump. The direction of the emission is the same as that of the pump field, that is, 3.8° from the growth direction (see Supplementary Information).

by the speed of the polaritons and the size of the pump spot. Figure 1c illustrates the dynamics of the propagation of the emission, calculated with the model described below. Fast propagation is essential for linking multiple consecutive switches in a single integrated device[14].

Our experiments were performed at 5 K in an InGaAs/GaAs/AlGaAs microcavity (see Methods). Both the pump and probe beams were c.w., focused on the sample in spots with diameters of 60 and 6 μm, respectively, with independent control of their polarization. Their angle of incidence on the microcavity was 3.8° (polariton in-plane momentum $k_p = 0.49$ μm^{-1}), and they had the same wavelength (836.95 nm), blue-detuned by 0.16 meV from the lower polariton branch state, as shown in the inset of Fig. 1a. Real-space images of the emitted intensity in transmission geometry were

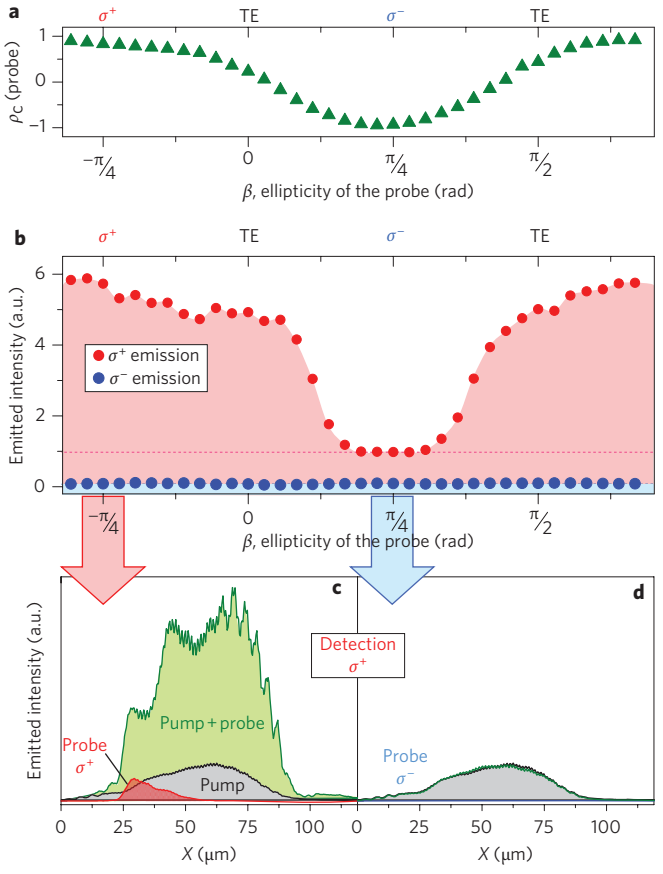

Figure 3 | Sensitivity to probe polarization. a, Variation of the degree of circular polarization of the probe alone ($\rho_c = (I^+ - I^-)/(I^+ + I^-)$, where $I^{+(-)}$ is the $\sigma^{+(-)}$ emission intensity) as a function of the input ellipticity, characterized by the parameter β (see Methods for a detailed description). The main polarization configurations (σ^+, σ^- and linear TE) are indicated in the upper part of the panel. **b**, Emitted intensity integrated over the pump area, excluding the probe arrival region, for a σ^+ pump and different polarization degrees of the probe. When the probe is σ^+ ($\beta = -\pi/4$) co-circularly polarized with the pump, a gain of almost six is obtained with respect to the pump-only case (red dotted line). When the ellipticity of the probe is within some narrow range around the cross-circularly polarized configuration ($\beta = \pi/4$), no gain is observed. **c**,**d**, σ^+ emission integrated over the vertical (y) direction in space with σ^+ ($\beta = -\pi/4$) and σ^- ($\beta = \pi/4$) probes, obtained from Fig. 2c and d, respectively.

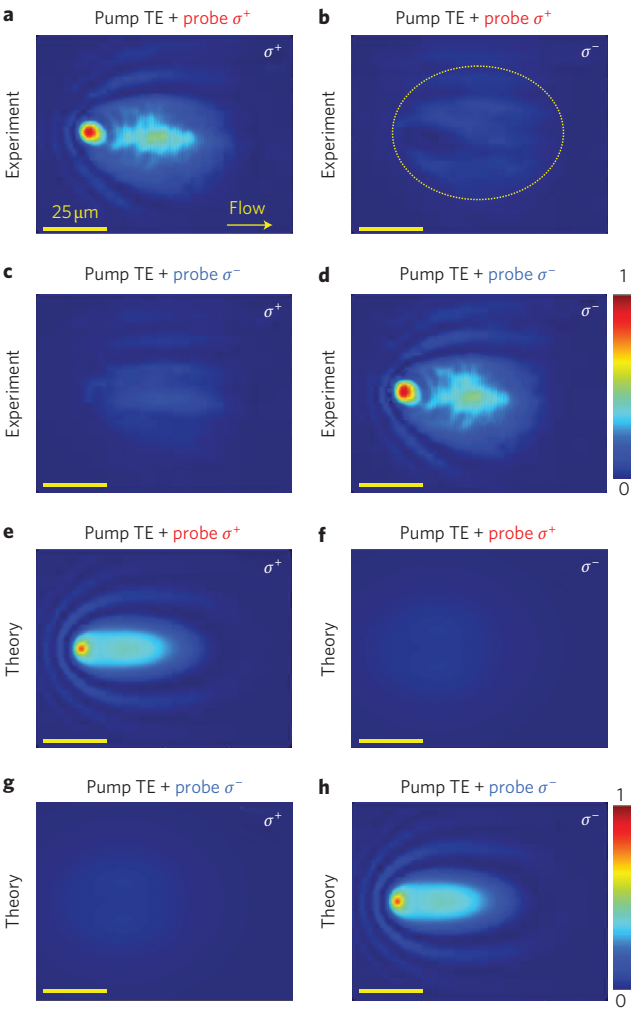

Figure 4 | Polarization propagation (TE pump). a–d, Real-space experimental images of the emitted intensity, resolved in the σ^+ (left column) and σ^- (right column) polarizations for the case of a linearly polarized pump. In the presence of a σ^+ circularly polarized probe (**a**,**b**), the emission of the whole spot becomes σ^+. When the sign of the circular polarization of the probe is inverted (σ^-; **c**,**d**), nonlinear absorption and emission occur with an inverted degree of circular polarization. **e–h**, Results from the numerical solution of the Gross–Pitaevskii equations corresponding to the experiments in **a–d**, respectively. The dotted line in **b** depicts the extension of the pump.

analysed regarding polarization and recorded by a charge-coupled device (CCD) camera. Simulations were performed by solving the spin-dependent Gross–Pitaevskii equation[14] for polaritons under c.w. pumping for the same pump/probe conditions as in the experiment (see Methods).

Figure 2 shows the operation of the conditional circular polarization optical switch. Here, the pump (Fig. 2a), with a power of 165 mW, is σ^+-polarized, injecting a polariton density corresponding to point I in Fig. 1a (off, total transmission 9.6 mW). The arrival of a σ^+-polarized (co-circularly) probe of 11 mW creates a surplus of spin-up polaritons, which drives the probed area to point II in the emission curve (on). The propagation mechanism described above drives the rest of the pumped area to the on nonlinear regime, preserving the σ^+ circular polarization and with a total transmission of 54 mW (Fig. 2c; polaritons move from left to right). In contrast, if the probe is σ^- (cross-circularly polarized), no change in the emitted intensity is observed (Fig. 2d). Figure 2e,f shows the corresponding simulated images, which are in close quantitative agreement with experiment.

The sensitivity of the spin switch to the polarization of the probe is explored in Fig. 3b for fixed pump and probe powers. The emission integrated over the pump area, excluding the probe arrival region, is shown (symbols) for different polarizations of the probe (parameter β, see Methods and Fig. 3a). When pump and probe are co-circularly polarized ($\beta = -\pi/4$), a strong gain of six is induced in the pump emission (Fig. 3c). As long as the surplus of probe polaritons co-circularly polarized with the pump is large enough to drive the system from I to II in Fig. 1a, the switching takes place. For the probe power considered in Fig. 3, only in a relatively narrow ellipticity range around the cross-circularly polarized configuration ($\beta = \pi/4$) is this surplus not enough, and the probe not able to induce switching (Fig. 3d).

A different situation can be achieved if the pump is linearly polarized (transverse electric, TE, in our experiments). In this case, the system can be considered to consist of two weakly interacting polariton gases with $s_z = +1$ and $s_z = -1$. The arrival of a

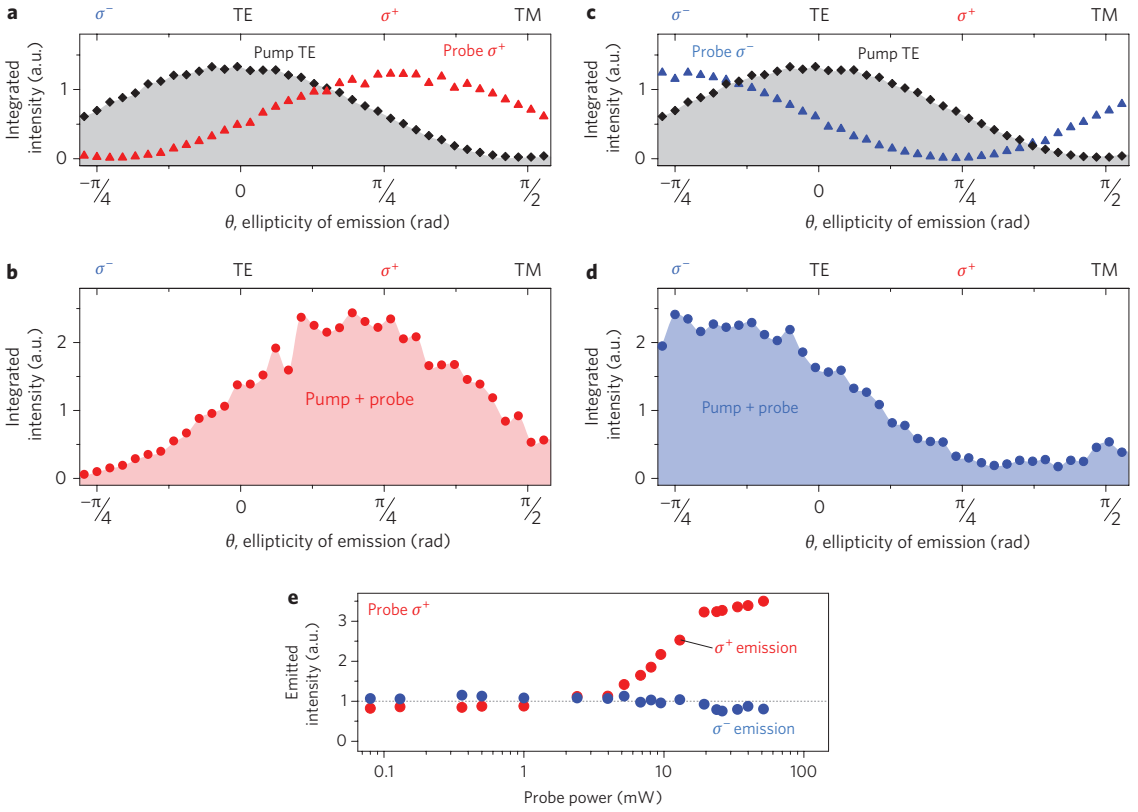

Figure 5 | Probe-controlled polarization. a, Integrated transmitted intensity of a linearly polarized TE pump only (black diamonds) and a σ^+ probe only (red triangles) for different detected ellipticities (see upper scales and Methods for a detailed description of θ). **b**, Emitted intensity when both pump and probe beams are simultaneously turned on, showing an emission centred on the σ^+ polarization (that is, that of the probe). **c**,**d**, Analogous data for a σ^- probe (blue triangles). In this case, when both pump and probe beams are turned on (**d**), the emission is centred on the σ^- polarization. The emission has been integrated over the whole spot for the case of the probe-only data (red and blue triangles), and in an area of 220 μm^2 in the centre of the spot for the case of the pump only (black diamonds) and pump plus probe (red and blue circles) data. The system is driven from a degree of circular polarization of the pump of 2% (that is, linearly polarized) to a value of up to 93% in the centre of the spot when the probe has switched on the system. **e**, Circular polarization resolved emission, in the conditions of pump plus probe, as a function of the power of a σ^+ probe (power of the pump: 145 mW). A threshold for the onset of bright emission with a polarization selected by the probe is clearly seen at 4.5 mW.

circularly polarized probe creates polaritons that switch the pump emission from point I to II in Fig. 1a, exclusively for polaritons with spin parallel to that of the probe, eventually propagating to the rest of the pump spot through the mechanism described above. This may be observed in Fig. 4a–d, which shows the polarization-resolved intensity when a circularly polarized probe interacts with a linearly polarized sub-threshold pump. One can see that the entire pump spot is switched into the on state, with the same circular polarization as that of the probe. Theoretical simulations (Fig. 4e–h) quantitatively reproduce these experimental results.

A detailed analysis of the polarization of the emission is presented in Fig. 5 for σ^+ and σ^- probes (panels a,b and c,d, respectively). The ellipticity of the emission can be characterized by the parameter θ, where $\theta = \pi/4$ ($-\pi/4$) corresponds to σ^+ (σ^-) circular polarization, and $\theta = 0$ ($\pi/2$) to TE (TM, transverse magnetic) linear polarization. Figure 5a–d shows that the pump emission passes from linear TE polarization in the off state (black symbols), to circular with the same orientation as that of the probe in the on state (Fig. 5b,d).

The polariton nonlinearities in this work were so high that our switches needed very low excitation densities to operate. For this reason we were able to perform all the experiments in the c.w. regime, without the need for pulsed excitations with large peak powers as are usually required in all-optical switches[1]. Figure 5e demonstrates a probe power threshold as low as 4.5 mW for the switch on of the whole pump spot, which had a diameter of 60 μm and a power of 140 mW (1.75 kW cm^{-2}). The saturation of the polarization at high densities is consistent with our spin-dependent polariton–polariton interaction model (Fig. 1a).

If we consider the polariton lifetime of our microcavities (5 ps) and the above-mentioned pump and probe excitation densities for switching operation, we estimate an upper limit for the switching energy of 1 fJ μm^{-2} (100 nJ cm^{-2}), two orders of magnitude lower than in state-of-the-art all-optical spin switches[1,9]. Meanwhile, the speed of the non-local action is given by the polariton propagation velocity[19,25] v_p, which is ~0.94 μm ps^{-1} in our experiments (calculated from $v_p = \hbar k_p/m$, where k_p and m are the polariton momentum and mass, respectively). With such speed, polaritons cross the entire spot in ~60 ps, inducing the commutation to the on state (see right panel in Fig. 1b). This corresponds to an on/off repetition rate of 10 GHz for such a big spot. We expect that this value can be further increased by increasing the polariton momentum by pumping with a higher angle of incidence[19,25].

Let us comment on the feasibility of extending our results, obtained at a temperature of 5 K, to room temperature. At room temperature, strong coupling has been observed in GaAs/InGaAS microcavities[29], and strong coupling together with nonlinear emission has been demonstrated in GaN-based microcavities[30]. Although nonlinear interactions have to be evaluated in the former case, and sample quality still needs to be improved in the latter case to allow for the

long-distance propagation of polaritons, these elements contribute to the significant potential for extending spin switching to temperatures higher than 5 K and to room temperature.

In conclusion, we have demonstrated the feasibility of light polarization conditional switches and polarization propagators, based on a pump and probe scheme in a semiconductor microcavity. A localized trigger is able to switch on a large pump area and to control the polarization of the full emission. The non-local action is based on the spin-dependent nonlinear polariton interaction and fast polariton propagation. Compared to conventional photonic switches, our device has several important advantages: its micrometre size and non-local action and, most importantly, the fact that it allows for operation with polarization-encoded signals. These schemes are key to the realization of 'polariton neurons', the building blocks of all-optical integrated logic circuits based on exciton–polaritons[14].

Methods

Sample description. Our system is a 2λ GaAs microcavity containing three $In_{0.04}Ga_{0.96}As$ quantum wells with a thickness of 80 Å placed at the maxima of the electromagnetic field of the cavity mode. The Bragg mirrors embedding the cavity are formed by 21 and 24 pairs of $Al_{0.1}Ga_{0.9}As$/AlAs layers, with reflectivities between 99.85% and 99.95%. The strong coupling between the exciton and cavity modes is obtained with a normal-mode Rabi splitting of 5.1 meV at 5 K, with polariton linewidths on the order of 0.1 meV. The microcavity was grown with a wedge in the cavity spacer to allow for the selection of the photon–exciton energy detuning simply by choosing the excitation point in the sample. However, in this work, all experiments were performed at the same point on the sample, corresponding to photon–exciton detuning of about +2 meV.

Characterization of the polarization of the emission (θ) and of the probe (β). In Fig. 5a–d, the emission is resolved into different polarization ellipticites by making use of a combination of a quarter wave plate, a half wave plate and a linear polarizer, in which the half wave plate is rotated by an angle θ. The time-dependent part of the electromagnetic field can be characterized by the parameter θ, where the electric field amplitude along the TE and TM directions (corresponding to the electric field amplitudes along the X and Y directions set by the linear polarizer) has the form

$$E_{\mathrm{TM}} = A_0 \sin(\theta)\cos(\omega t)$$

$$E_{\mathrm{TE}} = A_0 \cos(\theta)\sin(\omega t)$$

With this definition, σ^+ (σ^-) polarized emission corresponds to $\theta = \pi/4$ ($-\pi/4$), and TE (TM) linear polarizations to $\theta = 0$ ($\pi/2$). Intermediate values describe different elliptical polarizations.

In Fig. 3a,b we explore the transmission under different ellipticities of the probe. In this case we include a quarter wave plate in the optical path of the probe, which is rotated by an angle β with respect to the linear polarization axis of the laser (TE), resulting in electric field amplitudes along the TE and TM directions, given by

$$E_{\mathrm{TM}} = A_0 \cos(\beta)\sin(\beta)[\cos(\omega t) + \sin(\omega t)]$$

$$E_{\mathrm{TE}} = A_0[\cos^2(\beta)\cos(\omega t) - \sin^2(\beta)\sin(\omega t)]$$

With this definition, excitation with a σ^+ (σ^-) polarized probe corresponds to $\beta = -\pi/4$ ($\pi/4$), and with a TE linear polarized probe to $\beta = 0, \pi/2$. Intermediate values describe different elliptical polarizations.

Spin-dependent Gross–Pitaevskii equation. When excited resonantly, polaritons behave as a coherent field, because their coherence time is much greater than their lifetime. An accurate theoretical description of polariton nonlinear dynamics can therefore be made using the mean-field approximation, which leads to the Gross–Pitaevskii equation (equivalent to the nonlinear Schrödinger equation). Including the spin degree of freedom, the Gross–Pitaevskii equation is given as

$$i\hbar\frac{\partial\psi_\sigma(\mathbf{x})}{\partial t} = \left(\hat{E}_{\mathrm{LP}} - \frac{i\hbar}{2\tau} + \alpha_1|\psi_\sigma(\mathbf{x})|^2 + \alpha_2|\psi_{-\sigma}(\mathbf{x})|^2\right)\psi_\sigma(\mathbf{x}) + f_\sigma(\mathbf{x}, t) \qquad (1)$$

The wavefunction or mean field, $\psi_\sigma(\mathbf{x})$, is a real-space ($\mathbf{x}$) two-dimensional field for which the index $\sigma = \pm 1$ represents one of two spin (circular) polarizations, t is time, and $\hat{E}_{\mathrm{LP}}$ is the kinetic energy operator, which should account for the non-parabolic dispersion of polaritons. The eigenvalues of $\hat{E}_{\mathrm{LP}}$ can be written in reciprocal space as

$$E_{\mathrm{LP}}(\mathbf{k}) = \frac{E_{\mathrm{C}}(\mathbf{k}) + E_{\mathrm{X}}(\mathbf{k})}{2} - \frac{\sqrt{\left[E_{\mathrm{C}}(\mathbf{k}) - E_{\mathrm{X}}(\mathbf{k})\right]^2 + \Omega^2}}{2} \qquad (2)$$

where E_{C} and E_{X} represent the bare cavity photon and exciton energies, respectively. For these we take parabolic dispersion relations, characterized by effective masses m_{C} and m_{X}. Ω represents the Rabi splitting. In equation (1), τ represents the polariton lifetime, and α_1 and α_2 the strength of polariton–polariton interactions in the triplet and singlet configurations, respectively. In the experiment, all polaritons are excited with a similar in-plane wave vector, which allows us to neglect any wave vector dependence of the polariton lifetime or interaction strengths. Finally, $f_\sigma(\mathbf{x}, t)$ represents the excitation of the system by a combination of time-dependent, polarized pumps and/or probes. We consider excitation with Gaussian pumps, with amplitude A_σ, energy $\hbar\omega$, and in-plane wave vector $\mathbf{k}_{\mathrm{p}}$:

$$f_\sigma(x, y, t) = A_\sigma e^{i\omega t} e^{-(x-x_{\mathrm{p}})^2/L_x^2} e^{-y^2/L_y^2} e^{i\mathbf{k}_{\mathrm{p}}\cdot\mathbf{x}} \qquad (3)$$

where L_x and L_y define the size of the spot, centred at $(x, y) = (x_{\mathrm{p}}, 0)$.

Our theoretical results come from the numerical solution of equation (1), with the initial condition $\psi_\sigma(\mathbf{x})|_{t=0} = 0$, and the following parameters: $\Omega = 5.1$ meV, $k_{\mathrm{p}} = 0.49\ \mu\mathrm{m}^{-1}$, $m_{\mathrm{C}} = 3 \times 10^{-5}\, m_{\mathrm{e}}$ (m_{e} is the free electron mass), $m_{\mathrm{X}} = 0.22 m_{\mathrm{e}}$, $\tau = 10$ ps, $\alpha_2 = -0.1\alpha_1$, $\hbar\omega - E_{\mathrm{LP}}(k_{\mathrm{p}}) = 0.16$ meV. The c.w. pump was characterized by $L_x = 42.5\ \mu$m, $L_y = 34\ \mu$m and $x_{\mathrm{p}} = 0\ \mu$m. The c.w. probe was characterized by $L_x = L_y = 2.5\ \mu$m and $x_{\mathrm{p}} = -15\ \mu$m.

Received 20 January 2010; accepted 3 March 2010; published online 4 April 2010

References

1. Wada, O. Femtosecond all-optical devices for ultrafast communication and signal processing. *New J. Phys.* **6,** 183 (2004).
2. O'Brien, J. L., Furusawa, A. & Vuckovic, J. Photonic quantum technologies. *Nature Photon.* **3,** 687–695 (2009).
3. Takahashi, R., Kawamura, Y. & Iwamura, H. Ultrafast 1.55 μm all-optical switching using low-temperature-grown multiple quantum wells. *Appl. Phys. Lett.* **68,** 153–155 (1996).
4. Liu, J. *et al.* Waveguide-integrated, ultralow-energy GeSi electro-absorption modulators. *Nature Photon.* **2,** 433–437 (2008).
5. Nishikawa, Y., Tackeuchi, A., Yamaguchi, M., Muto, S. & Wada, O. Ultrafast all-optical spin polarization switch using quantum-well etalon. *IEEE J. Sel. Top. Quantum Electron.* **2,** 661–667 (1996).
6. Takahashi, R., Itoh, H. & Iwamura, H. Ultrafast high-contrast all-optical switching using spin polarization in low-temperature-grown multiple quantum wells. *Appl. Phys. Lett.* **77,** 2958–2960 (2000).
7. Yildirim, M., Prineas, J. P., Gansen, E. J. & Smirl, A. L. A near-room-temperature all-optical polarization switch based on the excitation of spin-polarized 'virtual' carriers in quantum wells. *J. Appl. Phys.* **98,** 063506 (2005).
8. Yamamoto, N., Matsuno, T., Takai, H. & Ohtani, N. Circular polarization control in a silicon-based all-optical switch. *Jpn J. Appl. Phys.* **44,** 4749–4751 (2005).
9. Johnston, W. J., Prineas, J. P. & Smirl, A. L. Ultrafast all-optical polarization switching in Bragg-spaced quantum wells at 80 K. *J. Appl. Phys.* **101,** 046101 (2007).
10. Žutić, I., Fabian, J. & Das Sarma, S. Spintronics: fundamentals and applications. *Rev. Mod. Phys.* **76,** 323–410 (2004).
11. Martín, M. D., Aichmayr, G., Viña, L. & André, R. Polarization control of the nonlinear emission of semiconductor microcavities. *Phys. Rev. Lett.* **89,** 077402 (2002).
12. Gippius, N. A. *et al.* Polarization multistability of cavity polaritons. *Phys. Rev. Lett.* **98,** 236401 (2007).
13. Amo, A. *et al.* Collective fluid dynamics of a polariton condensate in a semiconductor microcavity. *Nature* **457,** 291–295 (2009).
14. Liew, T. C. H., Kavokin, A. V. & Shelykh, I. A. Optical circuits based on polariton neurons in semiconductor microcavities. *Phys. Rev. Lett.* **101,** 016402 (2008).
15. High, A. A., Hammack, A. T., Butov, L. V., Hanson, M. & Gossard, A. C. Exciton optoelectronic transistor. *Opt. Lett.* **32,** 2466–2468 (2007).
16. Grosso, G. *et al.* Excitonic switches operating at around 100 K. *Nature Photon.* **3,** 577–580 (2009).
17. Leonard, J. R. *et al.* Spin transport of indirect excitons. *Nano Lett.* **9,** 4204–4208 (2009).
18. Vörös, Z., Balili, R., Snoke, D. W., Pfeiffer, L. & West, K. Long-distance diffusion of excitons in double quantum well structures. *Phys. Rev. Lett.* **94,** 226401 (2005).
19. Amo, A. *et al.* Superfluidity of polaritons in semiconductor microcavities. *Nature Phys.* **5,** 805–810 (2009).
20. Stevenson, R. M. *et al.* Continuous wave observation of massive polariton redistribution by stimulated scattering in semiconductor microcavities. *Phys. Rev. Lett.* **85,** 3680–3683 (2000).

21. Baas, A., Karr, J. P., Eleuch, H. & Giacobino, E. Optical bistability in semiconductor microcavities. *Phys. Rev. A* **69,** 023809 (2004).
22. Leyder, C. *et al.* Interference of coherent polariton beams in microcavities: polarization-controlled optical gates. *Phys. Rev. Lett.* **99,** 196402 (2007).
23. Bajoni, D. *et al.* Optical bistability in a GaAs-based polariton diode. *Phys. Rev. Lett.* **101,** 266402 (2008).
24. Leyder, C. *et al.* Observation of the optical spin Hall effect. *Nature Phys.* **3,** 628–631 (2007).
25. Freixanet, T., Sermage, B., Tiberj, A. & Planel, R. In-plane propagation of excitonic cavity polaritons. *Phys. Rev. B* **61,** 7233–7236 (2000).
26. Renucci, P. *et al.* Microcavity polariton spin quantum beats without a magnetic field: a manifestation of Coulomb exchange in dense and polarized polariton systems. *Phys. Rev. B* **72,** 075317 (2005).
27. Rosanov, N. N. *Optical Bistability and Hysteresis in Distributed Nonlinear Systems* (Fizmatlit, 1997).
28. Moloney, J. V. & Gibbs, H. M. Role of diffractive coupling and self-focusing or defocusing in the dynamical switching of a bistable optical cavity. *Phys. Rev. Lett.* **48,** 1607–1610 (1982).
29. Houdré, R., Stanley, R. P., Oesterle, U., Ilegems, M. & Weisbuch, C. Room-temperature cavity polaritons in a semiconductor microcavity. *Phys. Rev. B* **49,** 16761–16764 (1994).
30. Christmann, G., Butte, R., Feltin, E., Carlin, J.-F. & Grandjean, N. Room temperature polariton lasing in a GaN/AlGaN multiple quantum well microcavity. *Appl. Phys. Lett.* **93,** 051102 (2008).

Acknowledgements

This work was partially supported by the Agence Nationale pour la Recherche (GEMINI 07NANO 07043). T.C.H.L. was supported by National Centre of Competence in Research Quantum Photonics (NCCR QP), research instrument of the Swiss National Science Foundation (SNSF). A.V.K. acknowledges the support from the European Theoretical Spectroscopy Facility project no. 211956. A.B. is a member of the Institut Universitaire de France.

Author contributions

All authors contributed extensively to the work presented in this paper.

Additional information

The authors declare no competing financial interests. Supplementary information accompanies this paper at www.nature.com/naturephotonics. Reprints and permission information is available online at http://npg.nature.com/reprintsandpermissions/. Correspondence and requests for materials should be addressed to A.A. and A.B.